Future changes of atmospheric icing in Norway

Emilie C. Iversen[1], Bjørn Egil Nygaard[1], Øivind Hodnebrog[2], Kristian Ingvaldsen[1], Maria Sand[2], Øyvind Welgaard[3]

[1] *Kjeller Vindteknikk, Norconsult, Norway*
[2] *CICERO, Norway*
[3] *Statnett, Norway*

emilie.claussen.iversen@norconsult.com, bjorn.egil.nygaard@norconsult.com, oivind.hodnebrog@cicero.oslo.no, kristian.ingvaldsen@norconsult.com, maria.sand@cicero.oslo.no, oyvind.welgaard@statnett.no

Abstract— **Here we aim at projecting the future changes in atmospheric ice loads in Norway, by the use of regional downscaling of global climate model data. The analysis focuses on changes in extreme values of rime ice and wet snow loads, with the perspective of overhead power line design. Projections show increases in both icing types over large parts of Norway towards the end of the century, no matter the choice of future realization for greenhouse gas emissions.**

Keywords— ***Climate change, atmospheric icing, ice loads, OHL design, downscaling***

I. Introduction

Overhead lines (OHLs) are typically designed according to the current or historic climate, based on values provided in national codes derived from historic observations or model simulations. With global warming, the frequency and severity of extreme weather events as well as the mean state of the climate will change. Considering that OHLs are designed with the expected lifetime of about 70 years, climate change impacts on the design parameters should be considered.

In Norway, loads due to atmospheric icing is one of the main meteorological design parameters for OHLs due to the country's northerly location and its topography, including high elevation mountains and a long and exposed coastline. Norway has experienced some of the world's highest recorded ice loads on overhead power lines with measured values exceeding 300 kg/m [1].

There are two types of atmospheric icing that mainly impact the transmission lines in Norway; in-cloud or rime icing due to supercooled liquid cloud droplets that freeze once in contact with the cable, and wet snow icing, which is caused by heavy precipitation in the form of wet snow or sleet at temperatures just above freezing that sticks to the cable [1]. Rime icing typically occurs on elevated and exposed mountains, and particularly close to the coast where moist air masses are advected over land where temperatures are below freezing in winter. The mountainous regions along the western coastline of Norway are particularly exposed as the westerly North Atlantic flow causes large amounts of clouds when air is lifted over the topographic barriers. Wet snow icing typically occurs in the lowlands for temperatures just above freezing during winter storm events.

In Norway, projections from the Coupled Model Intercomparison Project phase 6 (CMIP6) [2] generally show rising temperatures and more humidity and precipitation in winter [3]. It is though difficult to project future ice loads based on available global- or coarse-scale climate projections, as the loads depend on meteorological variables in non-linear combinations, and due to the high geographic dependence. For areas experiencing wet snow icing, projections of warming could imply that more winter precipitation will fall as rain. However, for the same areas, projections of more intense precipitation might indicate larger maximum wet snow loads if temperature stays close to 0 °C during extreme events. For rime ice, projections of increased moisture content of the air might indicate larger ice loads. At high altitude sites, extreme ice loads might accumulate over weeks or months if temperature rarely exceeds 0°C. If temperature will exceed 0°C more frequently in a future climate, maximum ice loads could also decrease. For these reasons it is clear that climate projections of high spatial resolution as well as detailed treatment of cloud and precipitation physics are needed to meet the objective of assessing the future development of atmospheric ice loads on a regional scale, and furthermore to take this into account in OHL design.

This research is carried out within the Icebox R&D project, led by the Norwegian transmission system operator, Statnett. The research objective is to assess possible changes in design ice loads over Norway. The goal is to create maps of future return period values, for wet snow and for rime ice, to be used by Statnett in their operation and planning.

In this paper we will present the methodology used to achieve this objective, as well as some chosen results. The methodology involves regional downscaling of global climate model data, to obtain the necessary degree of resolution and detail. Two global climate models and three socioeconomic/concentration pathways (scenarios) are used to obtain a spread in climate sensitivity and future realizations, and thereby an indication of some of the uncertainty related to future projections. The paper is structured as follows: Section II presents the methodology, including selection of global climate models, the regional model configuration and downscaling, and a description of the icing model and extreme value estimation. Results are presented in section III, conclusions in IV and discussion in V.

II. Methodology

Global climate models (GCMs) are the only source available for predictions of future climate. Because they represent the whole globe and are computationally expensive to run, their resolution is relatively coarse (on the order of 100 km). This causes an unrealistic representation of topography and climate predictions which are averages for large geographic areas. Due to the strong topographic and geographic dependence of atmospheric icing, the GCM data is here dynamically downscaled to a finer resolution using a regional model. Dynamical downscaling ensures a full representation of physical and dynamical processes, which is

important for the relevant meteorological variables here. However, dynamical downscaling of GCM data to the required resolution is computationally demanding, and it is not feasible to perform such downscaling for a large ensemble of GCMs, and a selection must be made.

A. Selected global climate models

As circulation regimes and large-scale weather patterns exert a strong influence on regional weather conditions, and thereby atmospheric icing, it is of importance that we select GCMs which relatively well represent such for our region of interest.

Climate sensitivity is the global mean surface temperature response to a doubling of atmospheric CO_2 concentrations since pre-industrial times. Since impacts of climate change (e.g., on atmospheric icing) are largely determined by how much the Earth warms for a given increase in greenhouse gases, it is beneficial to choose GCMs that span a range of climate sensitivities.

Based on the above criteria, as well as suitability for downscaling with WRF, the two GCMs chosen are CESM2 [4] and MPI-ESM1-2-HR [5]. The two models also compare relatively well against ERA5 reanalysis of mean Arctic surface temperature during 1979-2014 [6]. Their differing climate sensitivity [7] is reflected in future projections of global mean surface temperature (Fig. 1, top), where CESM2 projects stronger global warming than the CMIP6 ensemble mean and MPI-ESM1-2-HR projects weaker warming. However, over our region of interest, the temperature evolution in MPI-ESM1-2-HR is closer to the ensemble mean while the CESM2 is among the models with weakest warming (Fig. 1, bottom). The reason for the weak warming in CESM2 is a phenomenon called the North Atlantic warming hole (NAWH), which is a region in the North Atlantic ocean showing a cooling trend, linked to a slowdown of the Atlantic meridional overturning circulation [8]. The warming hole in CESM2 is strong [9] and one of the strongest among the CMIP6 models.

To obtain an even larger span in future warming, three future realizations, based on a combination of Shared Socioeconomic Pathways (SSPs) and the Representative Concentration Pathways (RCPs), are downscaled with WRF, namely SSP1-2.6 (a sustainable future), SSP2-4.5 (middle of the road) and SSP3-7.0 (more pessimistic development trends) [10]. In SSP1-2.6, global CO_2 concentration will decline after about 2040, while it will stabilize in SSP2-4.5 after about 2080 and continue to increase in SSP3-7.0.

B. Regional model configuration and downscaling

The regional model WRF (Weather Research and Forecasting) [11] version 4.1.2 is used for dynamical downscaling of the GCM data. The model is set up with one domain (Fig. 2) with a horizontal resolution of 12 km and 32 vertical levels. Model parameterization choices are listed in Table I. The Thompson and Eidhammer microphysics scheme is chosen due to its explicit development and extensive testing for winter conditions [12, 13], in addition to its successful use in simulating atmospheric icing conditions [14-19]. A modification has been made to the scheme regarding the representation of melting snow, to ensure accurate predictions of wet snow icing [20]. No cumulus scheme is used, so convective precipitation is treated explicitly by the model

GCM data is used as initial and lateral boundary conditions to WRF. The historical simulations are initialized on September 1, 1988, and the first 16 months are considered spin-up and not part of the analysis. The future simulations are initialized on January 1, 2015, restarting from the historical simulations. Only boundary conditions, sea surface temperature and the greenhouse gas volume mixing ratios in the radiation schemes are changed for the future time periods.

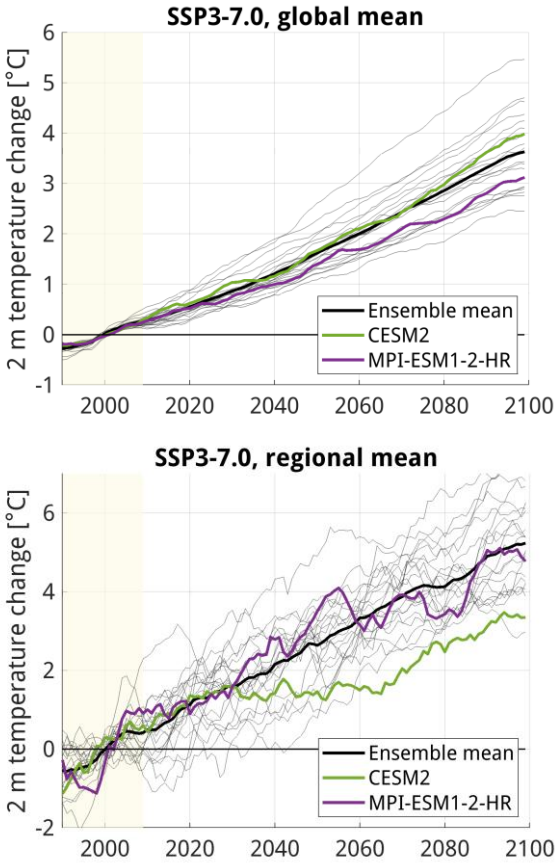

Fig. 1 Global (top) and regional (bottom) mean evolution of 2 m temperature anomalies relative to the mean of 1990-2009 (yellow shaded area) for the ensemble mean (black line) and individual (grey and colored lines) CMIP6 models for the SSP3-7.0 scenario. Each line shows 10-year moving averages for the winter season only (DJF). The regional means are approximately averaged over the WRF domain shown in Fig. 2.

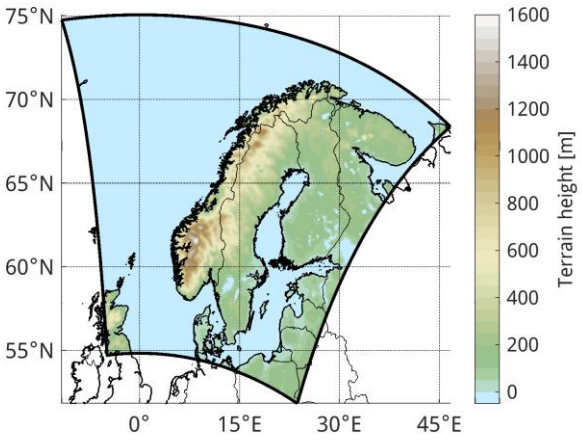

Fig. 2 Spatial extent and terrain height of the 12 km x 12 km resolution WRF domain.

TABLE I. PARAMETERIZATION SCHEME CHOICES FOR THE WRF MODEL CONFIGURATION.

Type of scheme	Name
Microphysics	Thompson-Eidhammer aerosol-aware [12]
Boundary layer	MYNN2 [21]
Radiation	RRTMG [22]
Land surface	Noah [23]

C. Icing model

Hourly outputs from the WRF simulations are used to generate time series of both wet snow and rime ice accretion for the whole WRF grid. Calculations of ice accretion are based on the model described in [24] which yields ice accretion rates on a reference cylinder. The two icing types are calculated separately. Our icing models also include melting and sublimation processes, and other features developed through extensive research and testing (see below).

For wet snow, the key WRF input variables to the icing model include temperature, air humidity, precipitation and wind speed. The temperature and air humidity are combined into one single variable, the wet-bulb temperature. This ice accretion model is also based on research by [17], with updates in several features from the ongoing Icebox project. The model now also allows for dry snow to accumulate, provided that the conductor is already covered with a layer of wet snow.

For rime ice, the key WRF input variables include temperature, wind speed, cloud water content and cloud droplet number concentration. For this icing type, an adjustment to the accretion model regarding the cloud droplet size distribution has been made, based on research within the Icebox project [25].

D. Extreme value estimation

Structural engineers deal with return periods and return values of climatic impacts when designing OHLs for a certain climate. A return value associated with the return period, p, is by definition the extreme value that is expected to be exceeded on average once every p years [26]. Here the focus will be on the 10-year return period of ice loads, and extreme value theory is used to fit suited distributions to our icing time series.

Wet snow icing typically occurs as well-defined, rare events, as it requires precipitation intensity above a certain threshold combined with air temperature within a narrow range. Therefore, the most suited extreme value method is Peaks-Over-Threshold (POT), which fits the ice load values that exceed a certain threshold to a generalized Pareto distribution. The threshold is selected so that the fit is optimal.

Rime ice will accumulate if temperature is negative and there are clouds present, implying typically long and sometimes uninterrupted icing events through the winter. Therefore, it is difficult to identify clear separate icing events, and yearly maximum values are used as input to the extreme value analysis (EVA). A Generalized Extreme Value (GEV) distribution is fitted to the yearly maximum values, where the shape parameter and associated distribution are customized to the data.

Although power lines are typically designed according to climatic loads with return periods of 50 years or greater, the present analysis is focusing on 10-year return period for several reasons: Given a dataset of 25 years, 10-year values are more robust compared to larger return periods whose values stem from the tail of the extreme value distribution. This is particularly important for a relatively rare phenomena like wet snow icing. Also, higher return period values will reflect more of the natural variability within that period, and as we want to extract a climate change signal, we want to eliminate as much of the natural variability as possible.

The common practice to separate a climate change signal from natural variability is to use projections from a large ensemble, such that natural variability is averaged out. Given our use of only two GCMs in this study due to the computational cost of dynamical downscaling, our results will contain significant natural variability. Another way to reduce natural variability is to perform spatial aggregation [27, 28]. Here we have applied spatial averaging, where the value of a grid cell results from averaging the 10-year return values from a matrix of 5 x 5 adjacent grid cells. This method was compared with the use of spatial pooling, where the extreme values of the 5 x 5 grid cell "pool" was fit to an extreme distribution and the 10-year value was obtained. The two results were similar. In this way we will still maintain the most important topographical signal, while also smoothing out noise.

Statistical significance of change in return values are tested using a two-sample Kolmogorov–Smirnov test, where the distributions used for testing consists of the extreme values from the grid cell pool, one for the historic and one for the future climate. The test is performed for each grid cell. Although the pool consists of somewhat dependent samples, the extreme value distribution provided a good fit to the data, as revealed through the spatial pooling test.

III. RESULTS

In the following subchapters, data resulting from the downscaling of the global models, CESM2 and MPI-ESM1-2-HR, with the regional model WRF, and the icing calculations are presented. The datasets are hereafter referred to as WRF-CESM and WRF-MPI, and when relevant, with the associated SSP scenario.

A. Validation of historic climate

A validation of the simulated temperature and precipitation from the historic period (1990-2014) is performed with gridded observational data (E-OBS) [29]. As can be seen in Fig. 3 (b and c), both datasets are mostly colder than the observations over Norway, WRF-MPI more so than WRF-CESM. WRF-CESM displays a cold bias of about -0.5 to -2.5 ºC, but a small warm bias over eastern Norway, and WRF-MPI a bias of about -1.5 to -4 ºC. WRF-CESM temperature validates relatively well for winter, spring and fall (Fig. 3, a), when atmospheric icing mainly occurs. WRF-MPI is too cold throughout the year. For precipitation, both models are mostly too wet compared to the observations, WRF-CESM more so than WRF-MPI (Fig. 3, e and f). WRF-CESM shows a wet bias of 1 – 150%, with the largest bias occurring over elevated

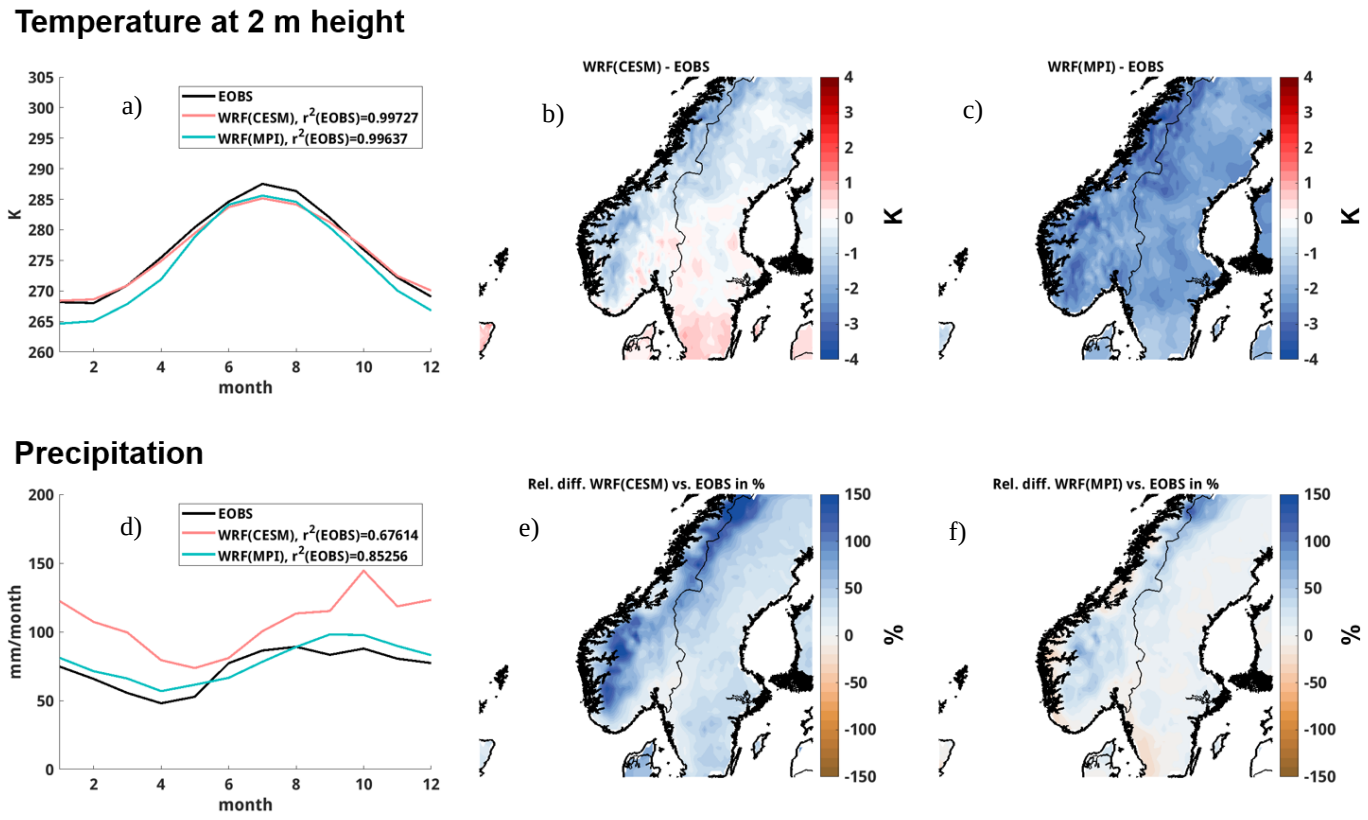

Fig. 3 Comparisons of the WRF-CESM and WRF-MPI historical periods (1990-2014) with gridded observations (E-OBS) of temperature (2 m; top) and precipitation (bottom). b) and e) are WRF-CESM and c) and f) WRF-MPI. The graphs in a) and d) are averaged over the spatial region (land only) shown in the maps.

areas. WRF-MPI shows a wet bias of about 1 – 100%, where the largest bias occurs over the northernmost part of the map. The wet bias over other elevated areas is restricted to about 75%. There is a relatively small (0 – 40%) dry bias along the coastline. For the icing season, it is clear that WRF-MPI validates best for precipitation (Fig. 3, d). It should be noted that the E-OBS data also contains biases; Hofstra, et al. [30] found a wet bias over large parts of southern and northern Norway (and dry bias in mid-Norway), which implies that the model wet biases in southern Norway could be even greater. However, Bandhauer, et al. [31] found a relatively good agreement between E-OBS precipitation and a high-resolution reference dataset. WRF has previously shown good performance in simulating climate over Norway [32], which is also the general experience of the authors through many years of application.

B. Future changes

In Norway, atmospheric icing mainly occurs between November and March, and so the winter season is further defined as this time span. Fig. 4 shows projected mean wintertime temperature for the downscaling simulations. The significant cold bias in the MPI model for our region (Fig. 3) causes the starting point of the WRF-MPI simulations to be roughly -3 ºC colder than the WRF-CESM simulations on average (Fig. 4, top). The WRF-MPI simulations with the two most moderate scenarios are still colder towards the end of the century than the historic period of WRF-CESM. Due to the NAWH, WRF-CESM generally shows a slower rate of warming compared to WRF-MPI, with warming levels of about 1.2, 1.7 and 2.5 ºC at the end of the century (respectively for increasing scenario), compared to 2.0, 2.7 and 4.4 ºC for WRF-MPI (Fig. 4, bottom). WRF-CESM-SSP126 shows the same rate of warming as WRF-MPI-SSP370 up to about 2040, implying similar absolute temperature as WRF-CESM-SSP370 at the end of the century, and a cooling after. WRF-CESM-SSP245 and WRF-MPI-SSP126 display minimal temperature change after roughly 2040 and 2050 respectively.

The large cold bias of the MPI model has a significant impact on the icing calculations (not shown), most likely leading to overestimated ice loads due to unrealistically long periods of freezing temperatures. Therefore, the focus of this paper will be on results from the WRF-CESM simulations (the results also from WRF-MPI will be published in a future paper). For each of the future realizations (SSPs), we divide the future timeline into three different periods, namely 2025-2049, 2050-2074, 2075-2099, to investigate changes in ice loads over time. Given the non-linear future development in temperature (Fig. 4) as well as non-linear dependence of atmospheric icing on temperature and precipitation/cloud water, we need to investigate at what point in time maximum ice loads are reached. This is important information for OHL design engineers to consider when planning for a certain future time horizon.

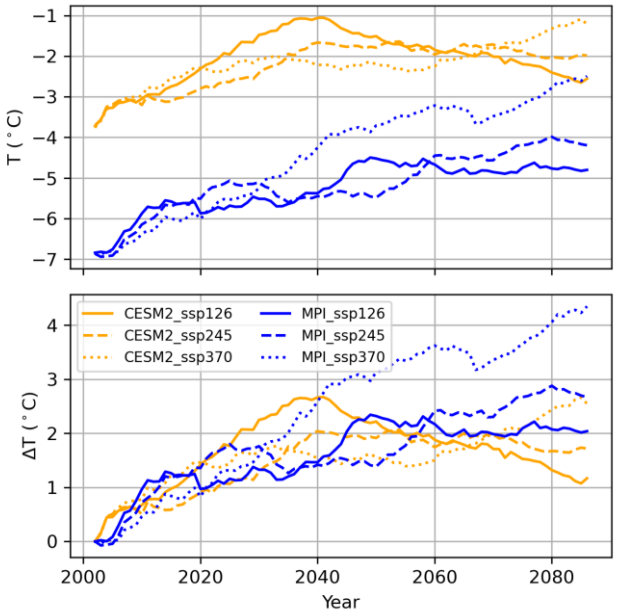

Fig. 4 Winter mean temperature evolution (top) and change (bottom) in WRF-CESM (orange) and WRF-MPI (blue) and the three scenarios (SSPs). 25-year moving averages, averaged over the landmass shown in Fig. 5decreasing .

1) *Wet snow*:

The main meteorological variables controlling wet snow icing are temperature and precipitation. Fig. 5 shows the future change in winter temperature (top) and precipitation (bottom) for the different scenarios and time periods over our region of interest. A prominent feature appearing in the temperature change field with time is the warming hole (NAWH), noticeable over ocean west of Norway. This, together with decreasing or stable global CO_2 concentrations for the SSP126 and SSP245 scenarios even cause a slight cooling in the latter period relative to the historic climate. As was seen in Fig. 4, temperature in the SSP126 scenario firstly increases rapidly, before cooling off, causing the earliest period to be considerably warmer than the latter, with temperature comparable to the latter period of SSP370.

The precipitation change pattern appears to be connected to the development of the NAWH, as the signal strengthens with the prominence of the warming hole. The early effect of warming on regional winter precipitation (2025-2049) is an increase over most of Norway, and a slight decrease southeast. As time progress the area of precipitation decrease expands, covering large parts of Norway in the latter period, except for southwest, south, and southeast. The most prominent area of precipitation decrease common in all scenarios is mid-Norway.

For changes in the 10-year return period of wet snow loads (Fig. 6) there seem to be a relatively strong agreement between scenarios and time periods. The general climate change signal of statistical significance (at the 0.9 level of confidence) is an increase in wet snow loads over the mountainous region in south-central and northern Norway (exceeding 3 kg/m for some parts, corresponding to 50 - 100 % (not shown)) and coastal areas of northern Norway (of roughly 1 kg/m, corresponding to 1 to 80 % depending on area), and a tendency of a decrease in coastal areas of southern Norway (of roughly 1 kg/m, corresponding to -1 to -50 % depending on area, but

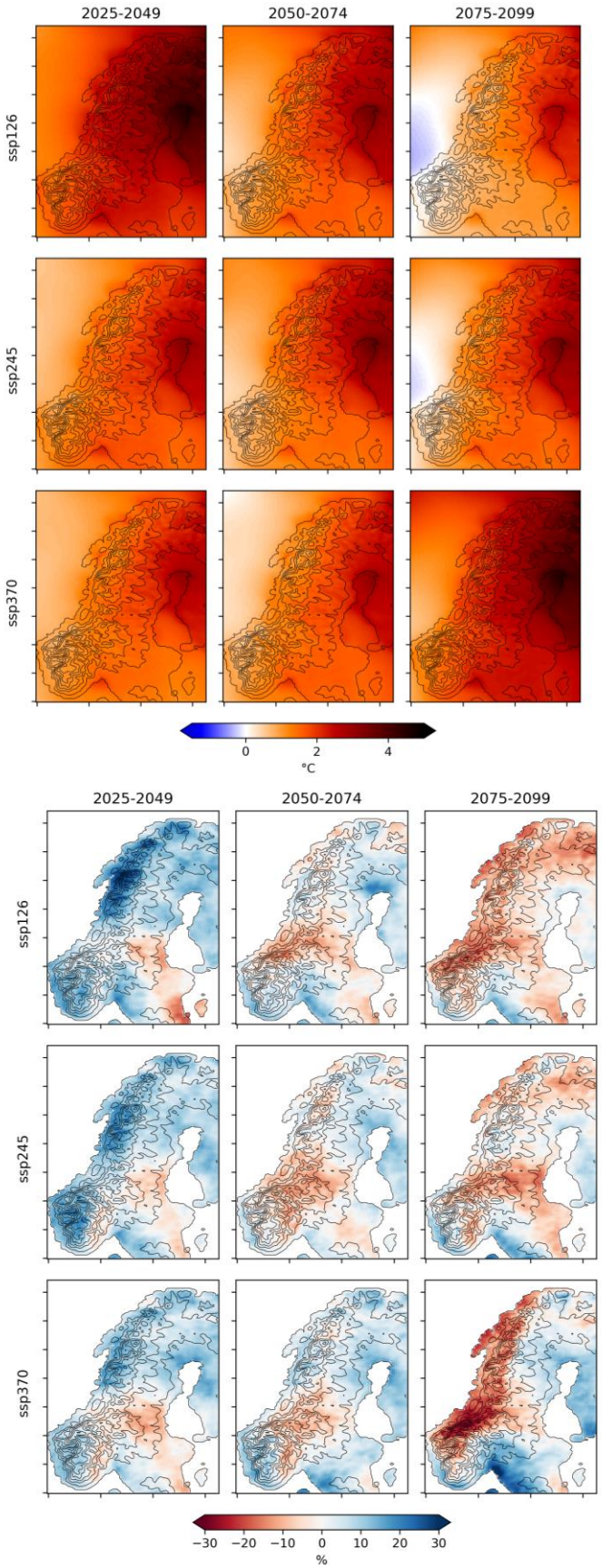

Fig. 5 Change in WRF-CESM winter mean temperature (ºC; top) and precipitation (%; bottom) between three different future periods and the historic period (1990-2014) for the three scenarios (SSPs).

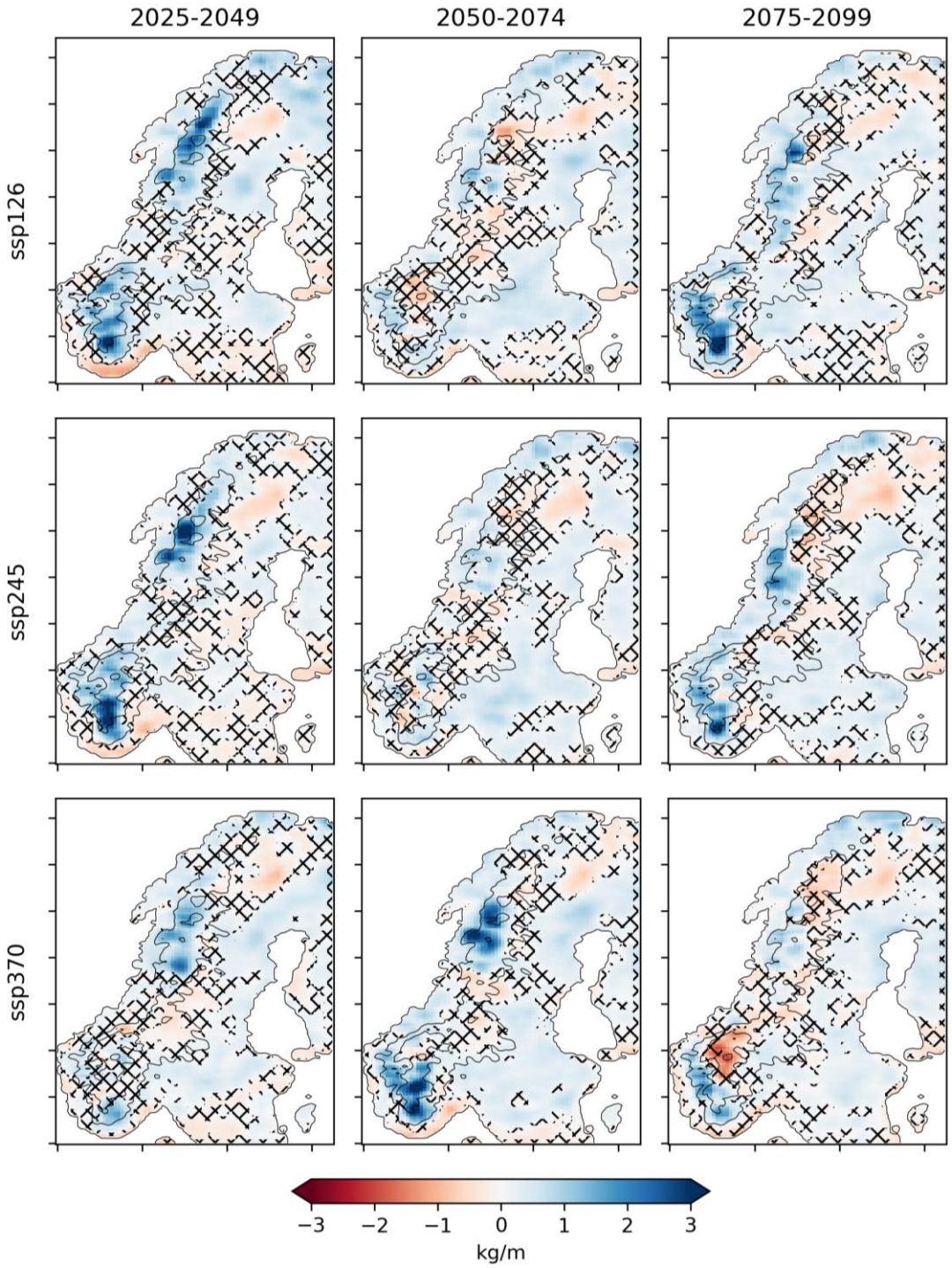

Fig. 6 Change in WRF-CESM 10-year return period of wet snow loads (kg/m) between three different future periods and the historic period (1990-2014) for the three scenarios (SSPs). Areas without hatching show a statistically significant change at the 0.9 level of confidence.

less consistent). In SSP126, where temperature is decreasing after ~2040, wet snow loads are increasing in this area. Varying sign of change and extent of significance can be seen over low-lying terrain in western and eastern Norway. It should be noted that for a rare phenomenon like wet snow loads of a considerable magnitude, natural variability in the model will influence the resulting signal to a relatively large degree, even though we have used the available tools (i.e. spatial pooling) to reduce such to the extent it is possible.

2) *Rime ice*:

The main meteorological variables controlling rime ice are temperature, cloud water content and wind. This study focuses on temperature and cloud water because the signal on changed wind speed is very weak and not significant. The response in cloud water content (Fig. 7) seems to be connected to the regional temperature response to a large degree. Generally, cloud water is increasing over elevated areas and decreasing in the lowlands, and the periods/scenarios with the largest cloud water increase corresponds with those of the largest

temperature increase (Fig. 5, top). As the warming hole develops, an area of decreasing cloud water becomes increasingly evident over the north-western part of the southern half of Norway (Møre and Romsdal County) and the coastline of northern Norway.

Change in 10-year rime ice loads (Fig. 7) cannot be directly inferred from the change in temperature and cloud water only, but is rather a result of the change in melting period frequency, duration of icing events, in combination with the change in cloud water content. For the earliest period there is an agreement between the scenarios of decreased ice loads over the mountainous area of Møre and Romsdal County of about -8 to -10 kg/m (or -20 to -60 %), which is statistically significant (with varying extent). Scattered areas of significant decreases are also found further north (-2 to -6 kg/m, -20 to -60 %). For the period 2050-2074 the remaining area of scenario agreement of significant decrease is a part of mid-Norway (Trøndelag County), most prominent in SSP245. In this scenario there is also still a significant decrease to the north. In this period there is also scenario agreement of a significant increase (with varying extent) in ice loads over the mountainous region of south-central Norway (5 to 10 kg/m, 20 to 60 %). Furthermore, in SSP370 there is an indication of a significant increase in ice loads in northern Norway. In the latter period the area of scenario agreement of significant increase in south-central Norway is expanded, and 10-year return period ice loads are further increasing. The increase is largest in the two most moderate scenarios (where temperature relative to the historic climate is cooling off the coast), with more than 10 kg/m for some parts (60 to 100 %, or exceeding 100 % over the westernmost part of this area). In these two scenarios the mountainous region of Møre and Romsdal County also experiences significantly increased loads. There is a tendency for an agreement of increased loads in northern Norway also, though only of statistical significance for the SSP126 scenario.

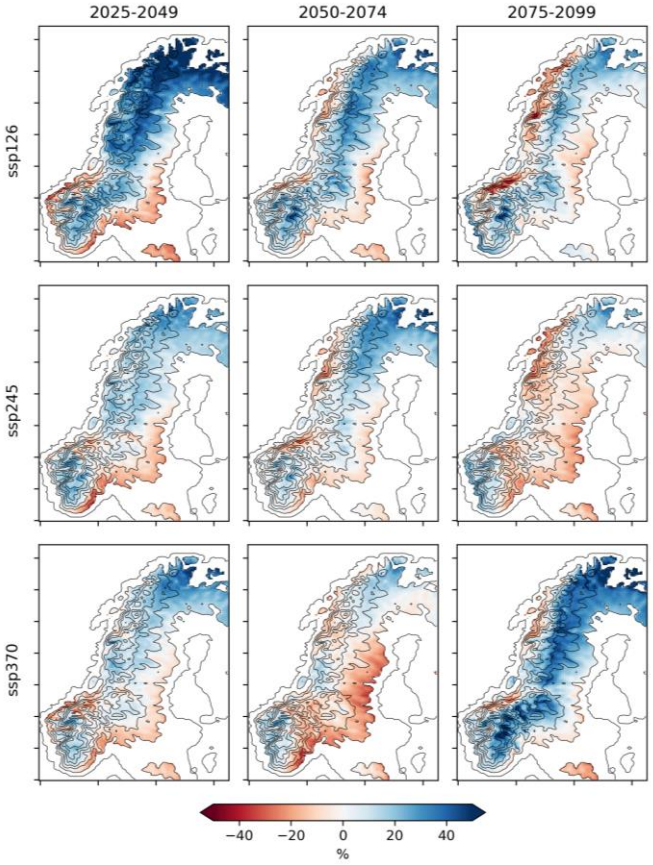

Fig. 7 Change in WRF-CESM winter total cloud water content (%) between three different future periods and the historic period (1990-2014) for the three scenarios (SSPs). Shown for terrain heights above 100 masl.

IV. Conclusions

OHLs are typically designed and built to withstand climatic impacts with a time horizon of 70 years. This means that ongoing or near-future OHL build projects must consider possible changes in climatic loads up to 2100. Although our results based on the downscaling of the CESM2 climate model contain great natural variability, some general conclusions about the future development of design ice loads can be drawn from this:

- Projections of rime ice loads and wet snow loads show increases over large parts of Norway towards the end of the century, no matter the choice of future realization for greenhouse gas emissions and world development.
- The mountainous region of south-central Norway shows statistically significant increases of 10-year values in all scenarios for both icing types, exceeding 10 kg/m in the most exposed parts (or more than 100 %) for rime ice, which is the dominating icing type at these elevations.
- Wet snow is often the dominant icing type in lower altitude terrain, showing statistically significant increases in large parts of northern Norway in all scenarios and periods (10-year values exceeding 4 kg/m, or 100 %, for some parts).
- For low-lying areas of the southern half of Norway, the wet snow climate signal is not clear, but the results indicate reductions along the coast and increases further inland.

With respect to near-future climate change and re-evaluation of existing OHLs design, we can also draw some conclusions based on our simulations for the period 2025-2049:

- The results indicate that there is no urgent risk of increased rime ice loads in high elevation terrain.
- All scenarios show statistically significant decreasing 10-year rime ice loads over large parts of northern Norway and over the mountains in Møre and Romsdal, and Trøndelag County (mid-Norway).
- The mountainous region of south-central Norway shows no significant change for rime ice, and the scenarios disagree on the sign of change.
- For wet snow, predictions of statistically significant increases in low-lying areas of northern Norway in this near-future period might indicate a need for design re-evaluation, though the predicted changes are relatively small (roughly 1 to 2 kg/m but corresponds to up to 70 % for some parts).
- The results regarding wet snow loads in low-lying areas of western, southern and eastern Norway are unclear.

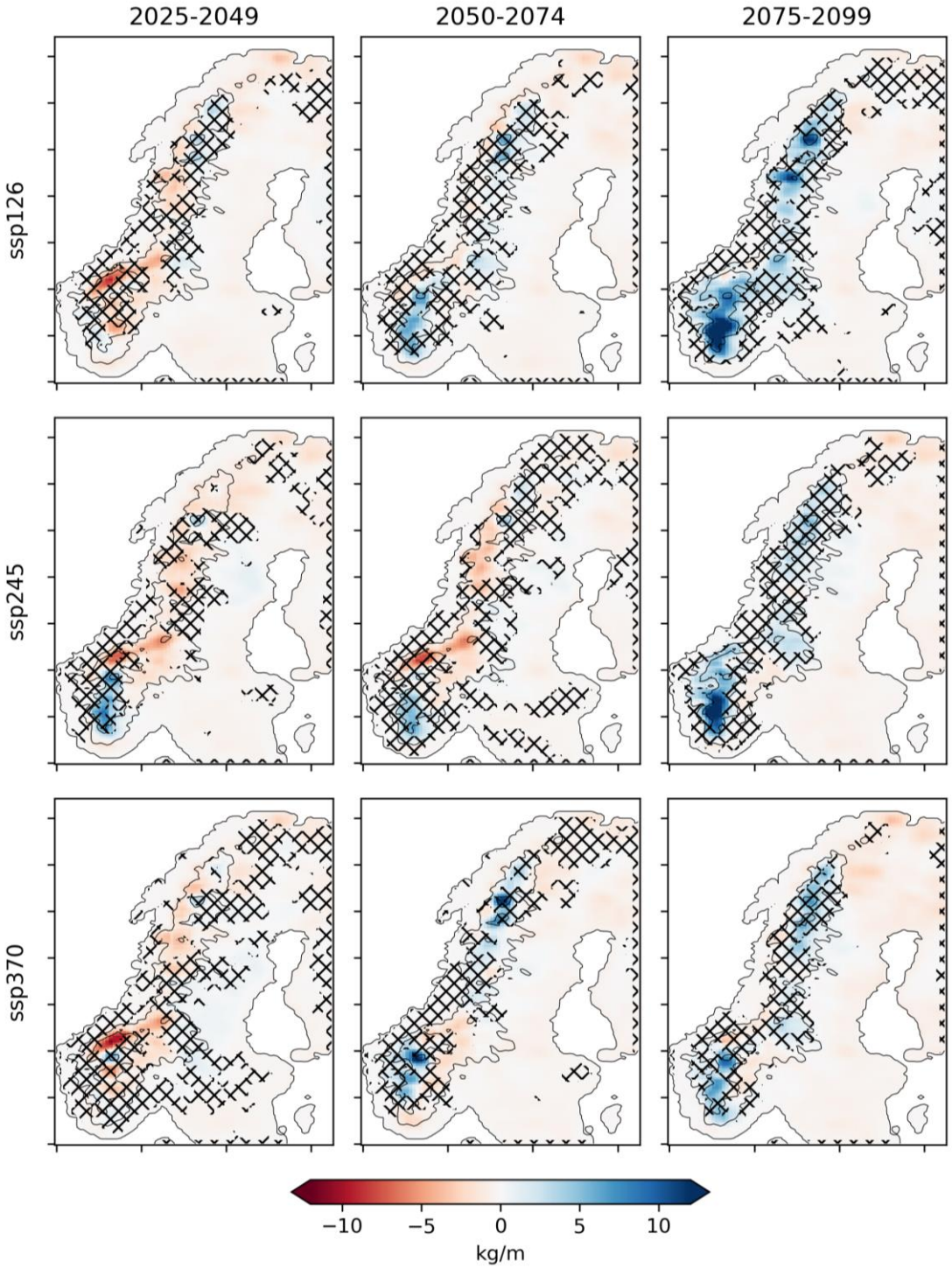

Fig. 8 Change in the WRF-CESM 10-year return period of rime ice loads (kg/m) between three different future periods and the historic period (1990-2014) for the three scenarios (SSPs). Areas without hatching show a statistically significant change at the 0.9 level of confidence.

V. Discussion

These results are based on projections from only one climate model. Single climate model future projections contain natural climate variability, which is particularly large at these latitudes [33]. The focus on a relatively small region (Norway), and also regional differences within the country, as opposed to large region averages, makes natural variability particularly prominent [27]. Significant natural variability (noise) implies a small signal-to-noise ratio when extracting a climate change signal from the simulations. Normal practice is to use a large climate model ensemble to average out natural variability. As high resolution and dynamical downscaling was needed in this study, the use of many climate models was not feasible. Although spatial averaging is performed to remove some of the natural variability, the results will still be affected to some degree. The use of statistical significance testing helps in identifying regions where the climate signal is robust.

As was discussed in Chapter II A, the regional response to global warming can differ greatly between different global climate models. The North Atlantic warming hole (NAWH) in CESM2 is one of the strongest among the CMIP6 models [9], significantly affecting future climate response over Norway and hence our projections of atmospheric ice loads. Even though CESM2 is a top-ranking model for many metrics for the relevant region [34], it is advised to combine realizations from a number of climate models to increase confidence in projections when evaluating the existing and planning the future powerline network. In further studies, the risk, cost and benefit of performing downscaling of additional climate models should be evaluated. As time progress it is also increasingly more certain which direction the world is going in terms of greenhouse gas emissions and world development, possibly eliminating some scenarios.

Regional downscaling of CMPI6 data is performed by various international modelling groups, and as more datasets become openly available, the assessment of future ice loads or other climatic loads and impacts can be performed, increasing confidence of predictions and reducing costs.

ACKNOWLEDGMENT

The authors would like to thank Statnett and the Norwegian Research Council for funding this work (project NFR 282403). Computing resources from Notur (NN9188K) and storage resources from Nird (NS9816K) are acknowledged

References

[1] S. M. Fikke, J. E. Kristjánsson, and B. E. Kringlebotn Nygaard, "Modern Meteorology and Atmospheric Icing," in *Atmospheric Icing of Power Networks*, M. Farzaneh Ed. Dordrecht: Springer Netherlands, 2008, pp. 1-29.

[2] V. Eyring *et al.*, "Overview of the Coupled Model Intercomparison Project Phase 6 (CMIP6) experimental design and organization," *Geosci. Model Dev.*, vol. 9, no. 5, pp. 1937-1958, 2016, doi: 10.5194/gmd-9-1937-2016.

[3] R. Ranasinghe *et al.*, "Climate Change Information for Regional Impact and for Risk Assessment Supplementary Material," in "Climate Change 2021: The Physical Science Basis. Contribution of Working Group I to the Sixth Assessment Report of the Intergovernmental Panel on Climate Change," 2021. [Online]. Available: http://www.ipcc.ch

[4] G. Danabasoglu *et al.*, "The Community Earth System Model Version 2 (CESM2)," *Journal of Advances in Modeling Earth Systems*, vol. 12, no. 2, p. e2019MS001916, 2020, doi: https://doi.org/10.1029/2019MS001916.

[5] W. A. Müller *et al.*, "A Higher‐resolution Version of the Max Planck Institute Earth System Model (MPI‐ESM1.2‐HR)," *Journal of Advances in Modeling Earth Systems*, vol. 10, no. 7, pp. 1383-1413, 2018, doi: 10.1029/2017ms001217.

[6] Z. Cai, Q. You, F. Wu, H. W. Chen, D. Chen, and J. Cohen, "Arctic Warming Revealed by Multiple CMIP6 Models: Evaluation of Historical Simulations and Quantification of Future Projection Uncertainties," (in English), *Journal of Climate*, vol. 34, no. 12, pp. 4871-4892, 01 Jun. 2021 2021, doi: 10.1175/jcli-d-20-0791.1.

[7] M. D. Zelinka *et al.*, "Causes of Higher Climate Sensitivity in CMIP6 Models," *Geophys. Res. Lett.*, vol. 47, no. 1, p. e2019GL085782, 2020, doi: https://doi.org/10.1029/2019GL085782.

[8] P. Keil, T. Mauritsen, J. Jungclaus, C. Hedemann, D. Olonscheck, and R. Ghosh, "Multiple drivers of the North Atlantic warming hole," *Nature Climate Change*, vol. 10, no. 7, pp. 667-671, 2020/07/01 2020, doi: 10.1038/s41558-020-0819-8.

[9] G. A. Meehl *et al.*, "Characteristics of Future Warmer Base States in CESM2," *Earth and Space Science*, vol. 7, no. 9, p. e2020EA001296, 2020, doi: https://doi.org/10.1029/2020EA001296.

[10] B. C. O'Neill *et al.*, "The Scenario Model Intercomparison Project (ScenarioMIP) for CMIP6," *Geosci. Model Dev.*, vol. 9, no. 9, pp. 3461-3482, 2016, doi: 10.5194/gmd-9-3461-2016.

[11] W. C. Skamarock *et al.*, "A Description of the Advanced Research WRF Version 4," NCAR Tech. Note, NCAR/TN-556+STR, 2019.

[12] G. Thompson and T. Eidhammer, "A Study of Aerosol Impacts on Clouds and Precipitation Development in a Large Winter Cyclone," *J. Atmos. Sci.*, vol. 71, pp. 3636-3658, 2014.

[13] G. Thompson, P. R. Field, R. M. Rasmussen, and W. D. Hall. (2008) Explicit Forecasts of Winter Precipitation Using an Improved Bulk Microphysics Scheme. Part II: Implementation of a New Snow Parameterization. *Mon. Wea. Rev.*, *136*. 5095-5115.

[14] Á. J. Elíasson, S. P. Ísaksson, H. Ágústsson, and E. Thorsteins, "Wet-snow icing: Comparing simulated accretion with observational experience," in *IWAIS 16th ed.*, Uppsala, 2015.

[15] A. Haldar, "Rime Icing Model Validation Using WRF and Full Scale Field Icing Data," CEATI, Montreal, 2016.

[16] B. E. Nygaard, J. E. Kristjánsson, and L. Makkonen. (2011) Prediction of In-Cloud Icing Conditions at Ground Level Using the WRF Model. *J. Appl. Meteor. Climatol.*, *50*. 2445-2459.

[17] B. E. K. Nygaard, H. Ágústsson, and K. Somfalvi-Tóth. (2013) Modeling wet snow accretion on power lines: improvements to previous methods using 50 years of observations. *J. Appl. Meteor. and Climatol.*, *52*. 2189-2203.

[18] B. E. K. Nygaard, Ø. Byrkjedal, E. Iversen, M. Fredbo, H. Ágústsson, and Ø. Welgaard, "Development of a reliable modeling system for the calculation of rime ice loads on overhead transmission lines," presented at the IWAIS, 2017.

[19] G. Thompson, B. E. Nygaard, L. Makkonen, and S. Dierer, "Using the weather research and forecasting (WRF) model to predict ground/structural icing," in *IWAIS 13th ed.*, Andermatt, 2009.

[20] E. C. Iversen, G. Thompson, and B. E. Nygaard, "Improvements to melting snow behavior in a bulk microphysics scheme," *J. Atmos. Res.*, vol. 253, p. 105471, 2021.

[21] M. Nakanishi and H. Niino, "An Improved Mellor–Yamada Level-3 Model: Its Numerical Stability and Application to a Regional Prediction of Advection Fog," *Boundary-Layer Meteorol.*, vol. 119, no. 2, pp. 397-407, 2006.

[22] M. J. Iacono, J. S. Delamere, E. J. Mlawer, M. W. Shephard, S. A. Clough, and W. D. Collins, "Radiative forcing by long‐lived greenhouse gases: Calculations with the AER radiative transfer models," *J. Geophys. Res.*, vol. 113, no. D13103, 2008.

[23] K. Mitchell, "The Community Noah Land-Surface Model (LSM) " NOAA, Boulder, CO, 2005.

[24] L. Makkonen and E. P. Lozowski, *Numerical Modelling of Icing on Power Network Equipment*. Dordrecht: Springer, 2008.

[25] P. Sokolov and M. S. Virk, "Droplet distribution spectrum effects on dry ice growth on cylinders," *Cold Regions Science and Technology*, vol. 160, pp. 80-88, 2019/04/01/ 2019, doi: https://doi.org/10.1016/j.coldregions.2019.01.002.

[26] S. Coles, *An Introduction to Statistical Modeling of Extreme Values*, 1st ed. 2001. ed. London: Springer London : Imprint: Springer, 2001.

[27] L. D. Brekke and J. J. Barsugli, "Uncertainties in Projections of Future Changes in Extremes," in *Extremes in a Changing Climate: Detection, Analysis and Uncertainty*, A. AghaKouchak, D. Easterling, K. Hsu, S. Schubert, and S. Sorooshian Eds. Dordrecht: Springer Netherlands, 2013, pp. 309-346.

[28] E. J. Kendon, D. P. Rowell, R. G. Jones, and E. Buonomo, "Robustness of Future Changes in Local Precipitation Extremes," (in English), *Journal of Climate*, vol. 21, no. 17, pp. 4280-4297, 01 Sep. 2008 2008, doi: 10.1175/2008jcli2082.1.

[29] R. C. Cornes, G. Schrier, E. J. M. Besselaar, and P. D. Jones, "An Ensemble Version of the E‐OBS Temperature and Precipitation Data Sets," *Journal of geophysical research. Atmospheres*, vol. 123, no. 17, pp. 9391-9409, 2018, doi: 10.1029/2017JD028200.

[30] N. Hofstra, M. Haylock, M. New, and P. D. Jones, "Testing E-OBS European high-resolution gridded data set of daily precipitation and surface temperature," *Journal of Geophysical Research: Atmospheres*, vol. 114, no. D21, 2009, doi: https://doi.org/10.1029/2009JD011799.

[31] M. Bandhauer *et al.*, "Evaluation of daily precipitation analyses in E-OBS (v19.0e) and ERA5 by comparison to regional high-resolution datasets in European regions," *International Journal of*

Climatology, vol. 42, no. 2, pp. 727-747, 2022, doi: https://doi.org/10.1002/joc.7269.

[32] U. Heikkilä, A. Sandvik, and A. Sorteberg, "Dynamical downscaling of ERA-40 in complex terrain using the WRF regional climate model," *Climate Dynamics*, vol. 37, no. 7, pp. 1551-1564, 2011/10/01 2011, doi: 10.1007/s00382-010-0928-6.

[33] J. W. Hurrell, Y. Kushnir, G. Ottersen, and M. Visbeck, "An Overview of the North Atlantic Oscillation," in *The North Atlantic Oscillation: Climatic Significance and Environmental Impact*, 2003, pp. 1-35.

[34] I. R. Simpson, Bacmeister, J., Neale, R. B., Hannay, C., Gettelman, A., Garcia, R. R., Lauritzen, P. H., Marsh, D. R., Mills, M. J., Medeiros, B., Richter, J. H., "An Evaluation of the Large‐Scale Atmospheric Circulation and Its Variability in CESM2 and Other CMIP Models," *J. Geophys. Res.: Atmos.*, vol. 125, p. e2020JD032835, 2020.